AMERICAN JOURNAL OF PHYSICAL ANTHROPOLOGY 107:1–12 (1998)

Deposits of Different Origin in the Lungs of the 5,300-Year-Old Tyrolean Iceman

MARIA A. PABST[1]* AND FERDINAND HOFER[2]
[1]*Institut für Histologie und Embryologie Universität Graz, Graz, Austria*
[2]*Forschungsinstitut für Elektronenmikroskopie, Technische Universität Graz, Graz, Austria*

KEY WORDS analytical electron microscopy; energy-filtering TEM; minerals; Ötztal Alps; threshing residues

ABSTRACT Deposits in the lung of the Late Neolithic Tyrolean Iceman were studied with a combination of different methods of analytical electron microscopy. Numerous anthracotic areas with plentiful inhaled soot particles were found in the lung; these most probably derived from open fires in houses. Between the soot particles tiny mineral crystals (mainly muscovite) were identified, which may indicate that the Tyrolean Iceman lived in a muscovite-rich area. Furthermore, illite, quartz, and a plagioclase (andesine), which are also minerals in the crystalline rocks of the Ötztal Alps, were found. Additionally, organic material, which may represent inhaled threshing residues, was present in the anthracotic areas. As threshing residues and seeds in husk also were detected in the Iceman's belongings, some kind of rustic occupation seems probable. Outside of the anthracotic areas, vivianite and hydroxyapatite crystals were detected. Because of their separate location, and as vivianite is also described in the Iceman's skin, these minerals seem to have crystallized during his 5,300 years of storage in the high mountains. Am J Phys Anthropol 107:1–12, 1998.

In September, 1991, alpinists discovered a well-preserved human mummy in the Italian part of the Tyrolean Ötztal Alps near the Austrian border. The mummy was lying in a depression in the glacial region near the Hauslabjoch at an altitude of 3,210 m (Lippert and Spindler, 1991; Henn, 1992; Zissernig, 1992). The discovery was a sensation, as this freeze-dried corpse is that of a man who had lived in the Late Neolithic, 5,300 years ago (Seidler et al., 1992). It is one of the oldest human mummies ever found. Along with the mummy, remnants were found of his clothes, made from hide, leather, and grass (Barfield et al., 1992; Spindler, 1995; Wininger, 1995), which also contained pollen grains (Bortenschlager et al., 1992; Groenman van Waateringe, 1995), seeds (Barfield et al., 1992; Spindler, 1995), and insects (Gothe and Schöl, 1992). Additionally, a number of items made of raw material of animal and plant origin, and of stone and copper were detected (Egg, 1992). All these materials reflect the living and environmental conditions of the Tyrolean Iceman, also affectionately called "Ötzi."

For additional information about the living and environmental conditions of this Late Neolithic individual, we studied deposits in his lungs. We used a combination of different methods of analytical electron microscopy to obtain comprehensive information on the elemental composition of organic and amorphous or crystalline inorganic materials in the Iceman's lungs (Hofer and Pabst, 1998).

*Correspondence to: Prof. Dr. Maria Anna Pabst, Department of Histology and Embryology, University of Graz, Harrachgasse 21, A-8010 Graz, Austria.
E-mail: maria-anna.pabst@kfunigraz.ac.at
Received 5 December 1997; accepted 24 April 1998.

MATERIALS AND METHODS

Lung material from the Tyrolean Iceman was fixed in a mixture of 3% glutaraldehyde and 3% paraformaldehyde in 0.1 M cacodylate buffer for 3 days at 4°C, followed by a 2-hour fixation with 2% OsO_4 at room temperature and embedding in TAAB epoxy resin. Semithin sections were stained with toluidine blue. Ultrathin sections were cut with thicknesses ranging from 30 to 60 nm and mounted without additional support directly onto Cu- or Ni-grids. The sections used for elemental analyses usually were not stained with heavy metal compounds because this staining would interfere with some elements in elemental analysis. The ultrathin sections were characterized by a combination of transmission electron microscopy (TEM), electron energy loss spectrometry (EELS), energy dispersive x-ray spectroscopy (EDXS), energy filtering TEM (EFTEM), and electron diffraction. The instrument used for this investigation was a Philips CM20/STEM equipped with a Gatan imaging filter (GIF) (Krivanek et al., 1991, 1992; Gubbens and Krivanek, 1993). The microscope was operated at a high tension of 200 kV with an LaB_6 cathode. The spectra and the images were recorded with the slow-scan CCD camera (De Ruijter, 1995) integrated in the GIF (YAG scintillator crystal; 1024 $\times$ 1024 pixel array). To collect chemical information (especially on lighter elements), EEL spectra were acquired with the GIF operated in spectrum mode with a probe diameter of about 20 nm (TEM image mode) (Egerton, 1996). The spectra were quantified using procedures described elsewhere (Hofer, 1991). Additionally, energy-dispersive x-ray spectra were recorded using a Noran HPGe detector with an ultrathin polymer window, thus enabling the detection of the elements C to U.

The Gatan imaging filter is a very important extension of the analytical capabilities of analytical electron microscopy because it makes possible the acquisition of energy-filtered TEM images (Gubbens and Krivanek, 1993; Hofer et al., 1995). The main advantage of EFTEM is that the two-dimensional distribution of chemical elements can be measured at high spatial resolution (some nanometers) and with short acquisition times (Hofer et al., 1995). In a previous work, we demonstrated the use of EFTEM elemental mapping for characterizing deposits in human lung tissue (Hofer and Pabst, 1998). The elemental maps can be obtained by recording an energy-filtered TEM image at the energy of an element-specific ionization edge. However, since this image contains an unspecific background one has to subtract this background contribution in order to get the true elemental map.

To obtain an optimal signal-to-noise ratio (SNR) in the elemental maps, the experimental conditions were chosen as previously recommended (Berger and Kohl, 1993; Kothleitner, 1996). The background contribution to the image intensity was removed by two methods. For the acquisition of elemental maps (three-window method), two energy-filtered background images in front of the edge and one image at the ionization edge of the element of interest were acquired (Egerton, 1996). An extrapolated background image was calculated using the power-law model $I = A.E^{-r}$, where I is the intensity, E is the energy loss, and A and r are two fitting parameters. The background image is subtracted from the ionization-edge image, thus producing the elemental map. If the element of interest is present only in low concentration, the three-window method produces noisy images (Krivanek et al., 1993; Hofer et al., 1995). Therefore, we also calculated jump ratio images (two-window method) by dividing the post-edge image by a pre-edge image (Johnson, 1979; Hofer et al., 1995).

Electron diffraction was carried out to see if the deposits were crystalline or amorphous. The electron diffraction patterns of the crystalline particles were used to measure the lattice distances (d-values), which were matched with the d-values of known mineral phases from the powder diffraction file (International Centre for Diffraction Data, Swarthmore, PA, USA). Together with the elemental composition, which was derived from the EDX and EEL spectra, the deposits could be identified unequivocally.

RESULTS

Light microscopic sections of the lung of the Tyrolean Iceman show tissue areas with

different toluidine blue staining intensities and intermingled holes, but no typical lung tissue structures could be identified. However, the lung sections contain a large number of anthracotic areas (Fig. 1). The TEM investigations confirmed these results. Beside cross-striated collagen fibrils, no structures which are typical for lung tissue could be identified. Figure 2a shows the TEM image of an anthracotic area, revealing a large number of fine-grained particles.

In order to identify the deposit phases, we applied energy-filtering TEM. As in previous lung tissue characterizations (Hofer and Pabst, 1998), we recorded elemental maps for the elements carbon, silicon, and oxygen (Figs. 2b–d) to localize soot, silicate, and other oxide deposits, respectively. The carbon map (Fig. 2b) showed that these particles consist mainly of carbon (bright regions). The EEL spectrum (Fig. 3c) taken from carbon-rich particles shows that they consist of carbon only; the near edge fine structure of the C K ionization edge in Figure 3c is typical for amorphous carbon (Hofer and Golob, 1987). For comparison, an EEL spectrum was recorded from a specimen region without deposits (dashed curve). The C K edge is clearly lower than in the deposits, thus confirming the results of the carbon map (= carbon enrichments). Since these deposit particles are amorphous (there are no reflection spots in the electron diffraction pattern), we may assume that these particles are soot.

The silicon map (Fig. 2c) was recorded with the Si L_{23} ionization edge and highlights the silicon-rich deposits. The oxygen map in Figure 2d shows that oxygen-rich deposits are distributed between the soot particles. These oxide particles correspond to black regions in the carbon map (Fig. 2b) and largely correspond to bright regions in the silicon map. Study of the lung of a human reference body recently mummified by freeze drying (Hofer and Pabst, 1998) showed mineral crystals similar to those found embedded in the anthracotic areas between plentiful soot particles in the lungs of the Tyrolean Iceman (Fig. 2).

In order to characterize the large silicate particle visible in Figure 2a, we acquired

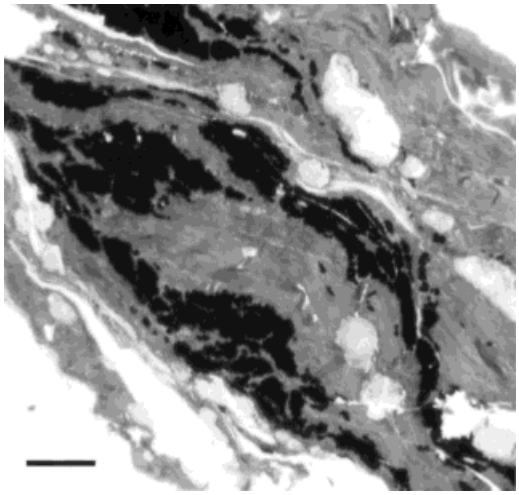

Fig. 1. Toluidine blue-stained semithin section of lung tissue from the Iceman containing several anthracotic areas seen as the darkest regions in the picture. Scale bar: 20 µm.

both an electron diffraction pattern and an EDX spectrum (Figs. 3a,b). The EDX spectrum (Fig. 3b) of the large deposit particle is characteristic for the mineral muscovite ($KAl_2(OH)_2AlSi_3O_{10}$), which was confirmed by the detailed analysis of the electron diffraction pattern shown in Figure 3a. Since the muscovite crystal is partially distorted by cutting, the reflections in the diffraction pattern are not typical for a single crystal and also contain features of a polycrystalline sample. All reflection spots could be indexed using the x-ray diffraction data of the muscovite structure.

The mica muscovite was the mineral most commonly found in the Iceman's lungs. Occasionally, we found large platy muscovite crystals a few µm long. However, the muscovite crystals were even more frequently found to be needle-shaped and only some tenths of a µm long. The latter crystals also contained a low concentration of iron.

Besides muscovite, we found feldspar particles with diameters of about 1 µm (Fig. 4a). Electron diffraction (Fig. 4b) and EDX spectrometry (Fig. 4c) showed that they are plagioclase. The EDX spectrum was quantified using the Cliff-Lorimer method (thin film approximation) (Cliff and Lorimer, 1975; Williams, 1987) and resulted in a mixing

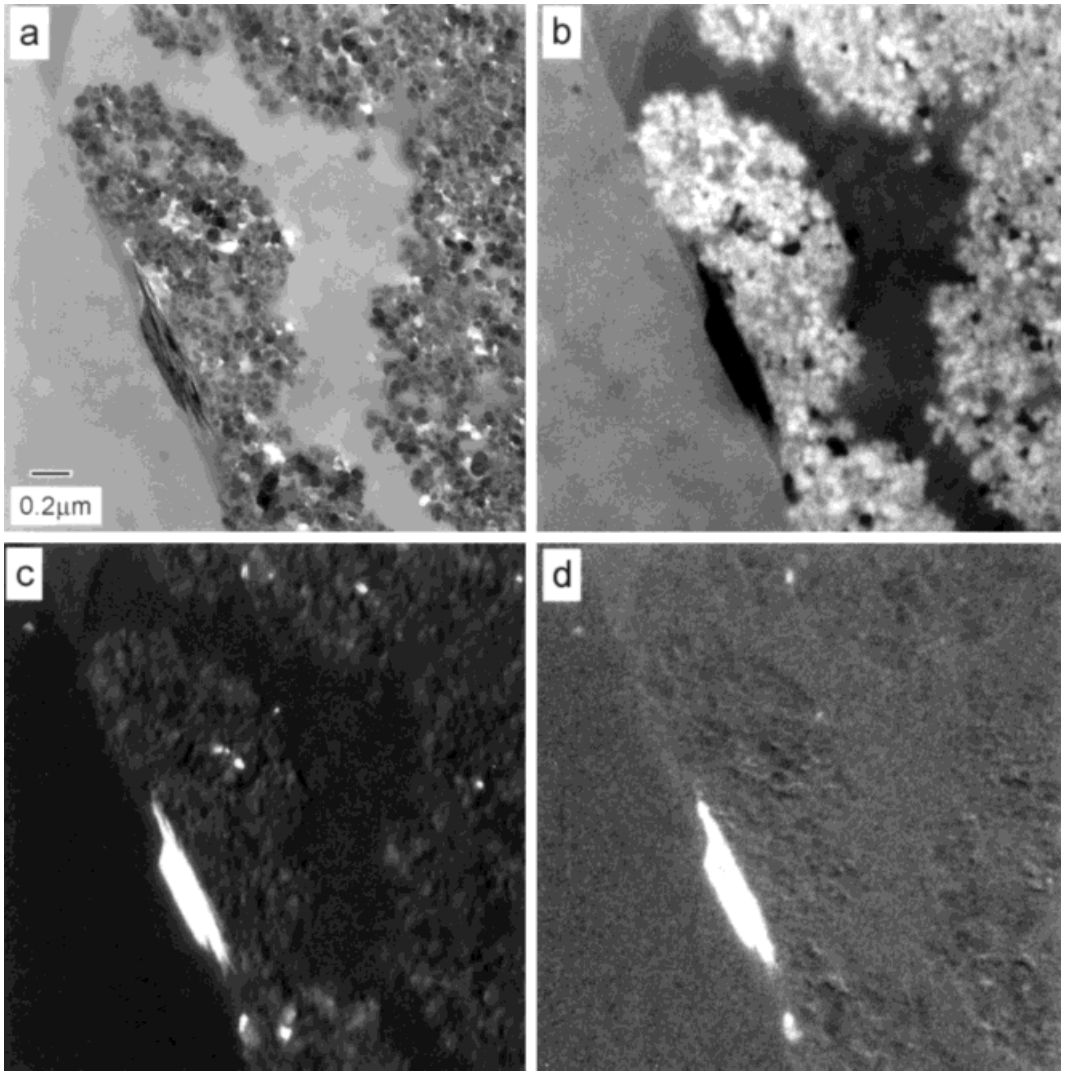

Fig. 2. Deposits in lung tissue imaged using the elemental mapping technique of energy-filtering TEM. (**a**) TEM bright field image of an anthracotic area. (**b**) Carbon elemental map showing the distribution of the soot particles. (**c**) Silicon and (**d**) oxygen elemental map showing the distribution of silicate particles.

ratio of about 60%:40% between albite $Na(AlSi_3O_8)$ and anorthite $Ca(Al_2Si_2O_8)$. Therefore, this phase is most probably andesine.

Additionally, platy crystals a few µm in size were found in the anthracotic areas (Fig. 4d). Using electron diffraction (Fig. 4e) and EDX spectrometry (Fig. 4f), these particles were identified as the clay mineral, illite $(K,K^+,H_3O^+)(Al,Fe,Mg)_2(OH)_2(Si,Al)_4(O,OH)_{10}$. The distinction between muscovite and illite was made, as stated above, by the combination of x-ray spectrometry and electron diffraction, where the latter method has the advantage that it enables an unequivocal identification. All the diffraction patterns of the crystalline phases have been completely indexed and compared with the data of the powder diffraction file; for a given compound all reflections had to be identified. These data from muscovite and illite, like the other investigated minerals, have been summa-

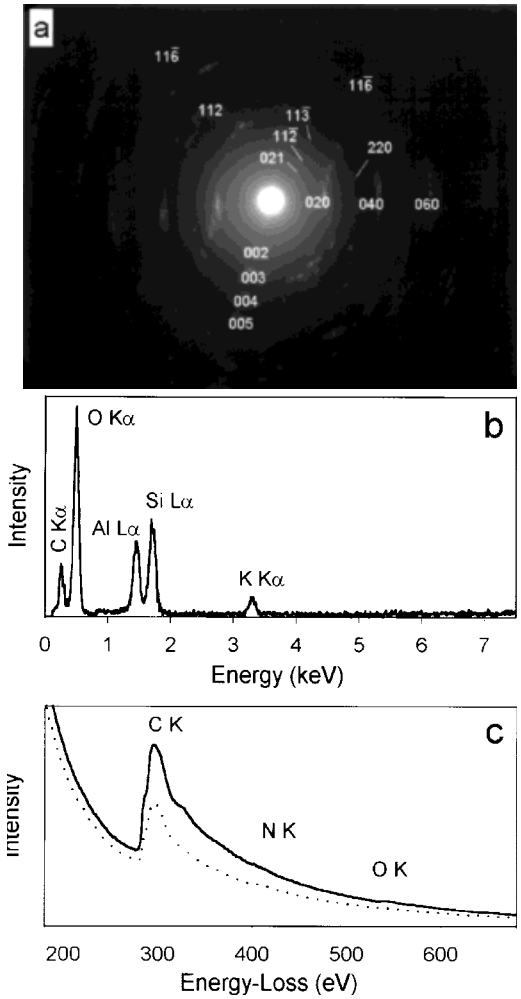

Fig. 3. (**a**) Electron diffraction pattern of the large mineral particle in Figure 2; the reflection spots have been indexed and correspond to the mineral muscovite. (**b**) EDX spectrum of the large particle shown in Figure 2 reveals elemental composition typical for the mineral muscovite, showing the element specific x-ray lines for Al, Si, K, and O. (**c**) EEL spectrum of a soot particle (solid) together with the EEL spectrum of a specimen region without deposits (dashed), showing the element-specific ionization edges for the elements C, N, and O (ionization of the K shells).

rized in tables which have not been included here.

The Tyrolean Iceman also inhaled some small quartz particles of some tenths µm in size (Figs. 5a–c).

Not only mineral particles were found in the anthracotic areas of the Iceman's lungs. There were also particles exhibiting a wide range of morphology and size. Figure 5d shows such a particle embedded in an anthracotic area with a diameter of some tenths of µm. Electron diffraction revealed that this particle is amorphous.

Electron energy loss- and EDX-spectrometry showed that this material consisted mainly of carbon and oxygen, sometimes with a small amount of silicon (Figs. 5e–f). The dark stripes in these particles probably derive from cutting, as this material seems to be harder than the surrounding tissue (Fig. 5d).

All the materials described so far were found in the anthracotic areas, sometimes embedded in and occasionally on the surface of the soot aggregates.

Besides these findings, there were also two kinds of crystalline compounds which were not found in these anthracotic areas, but were mainly deposited separately in the lung tissue. One of these materials is found as aggregates of small columnar iron phosphate crystals (Fig. 6a). EEL spectra, shown in Figure 6c, and electron diffraction patterns (Fig. 6b) show that it refers to vivianite $Fe_3(PO_4)_2 \times 8H_2O$ in an oxidized form (Gmelin, 1965). The quantification of the EEL spectrum gives a Fe to P ratio of 0.67 and a Fe to O ratio of 0.22; the latter is typical for oxidized vivianite and the near edge fine structure of the P L_{23} edge is characteristic of phosphate compounds (Hofer and Golob, 1987).

The second kind of crystal found separately in the lung tissue is hydroxyapatite $Ca_5(PO_4)_3OH$ (Fig. 6d). The crystals were found as tiny needles; the largest seen are about 100 nm long and about 7 nm wide. They were found grouped in areas with a diameter of a few µm, where they were arranged in a hexagonal pattern around organic structures (Fig. 6d). This phase was again identified with electron diffraction (Fig. 6e) and EEL spectrometry (Fig. 6f). Once more, the P L_{23} edge exhibits a fine structure which is typical for phosphates (Hofer and Golob, 1987).

These hydroxyapatite crystals were also found in round, dense aggregates (Fig. 7), up to 1.8 µm in diameter. In these aggregates, the crystals are found mainly in the form of tiny needles, as described above. Addition

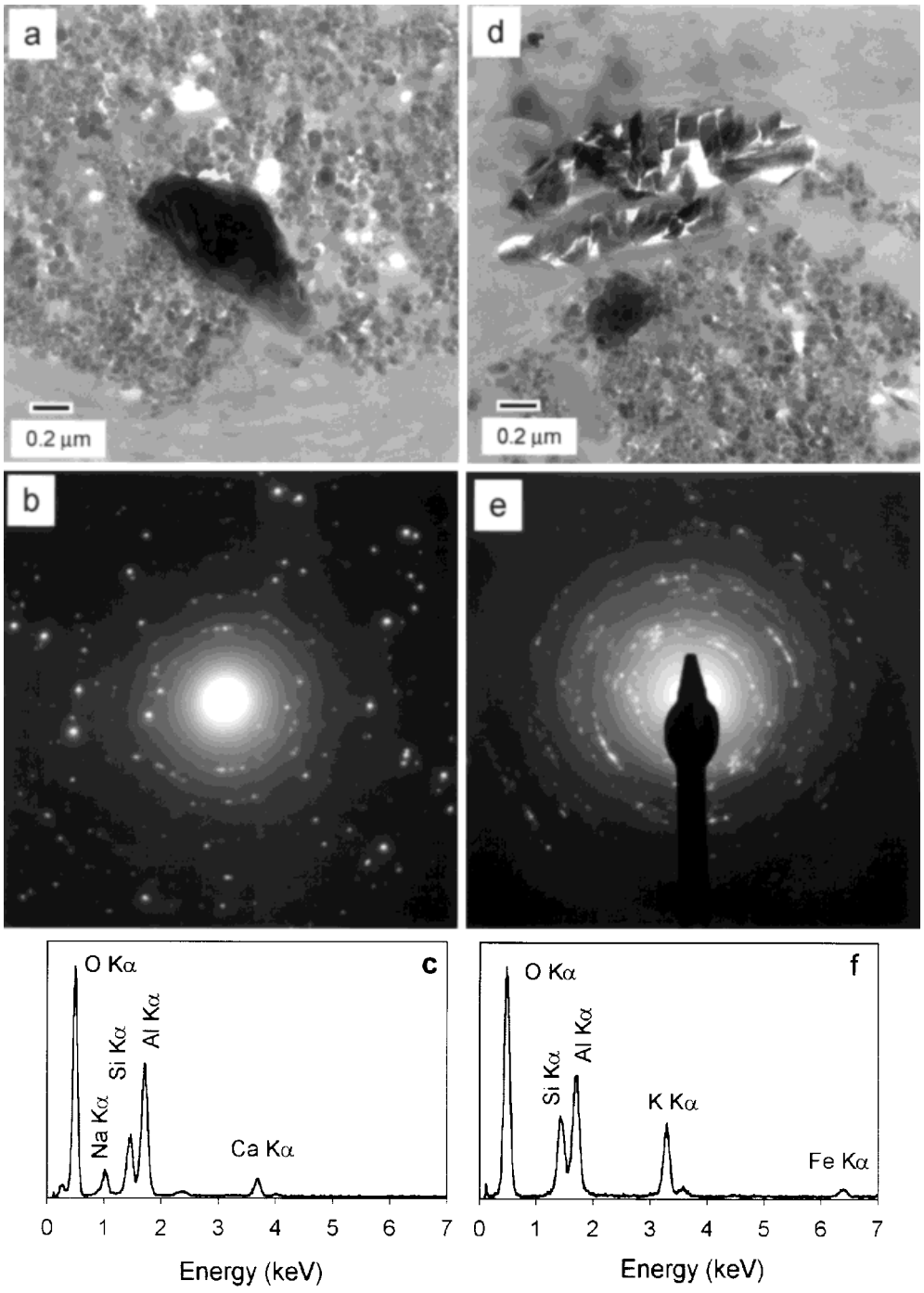

Fig. 4. Identification of deposits in an anthracotic area using TEM. (**a**) TEM bright field image of a mineral crystal identified by electron diffraction (**b**) and EDX-spectrometry (**c**) as plagioclase (element specific x-ray lines for Al, Si, Ca, Na, and O). (**d**) TEM image of a mineral crystal identified by electron diffraction (**e**) and EDX-spectrometry (**f**) as illite (element-specific x-ray lines for Al, Si, K, Fe, and O).

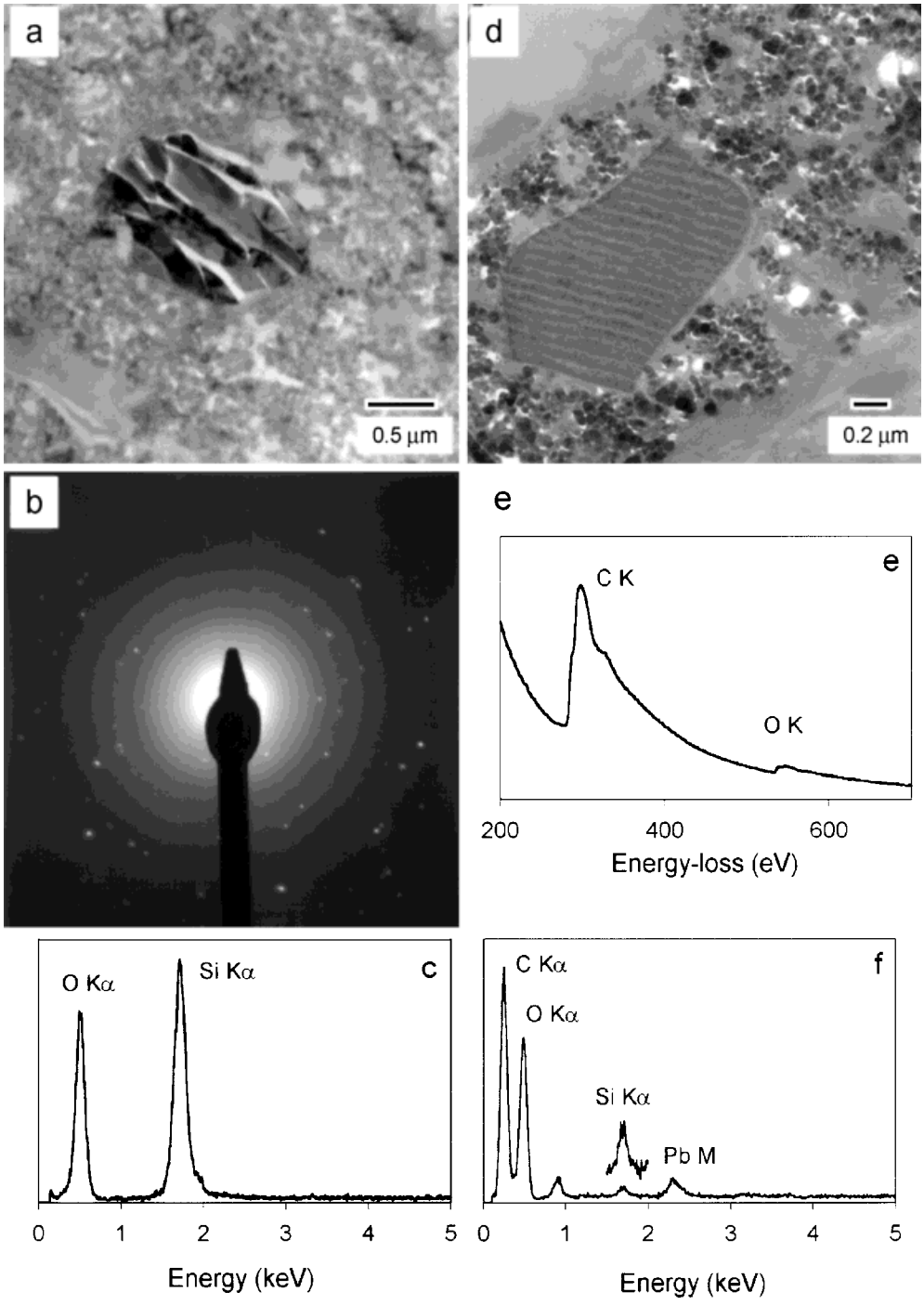

Fig. 5. Identification of deposits in an anthracotic area using TEM. (**a**) TEM image of a mineral crystal identified by electron diffraction (**b**) and EDX-spectrometry (**c**) as quartz (element-specific x-ray lines for Si and O). (**d**) TEM image of an often-found organic inclusion embedded in soot aggregates; the EEL spectrum (**e**) and EDX spectrum (**f**) of this particle. The spectra reveal the occurrence of carbon, oxygen, and a small amount of silicon. The Pb M edge derives from staining of this section.

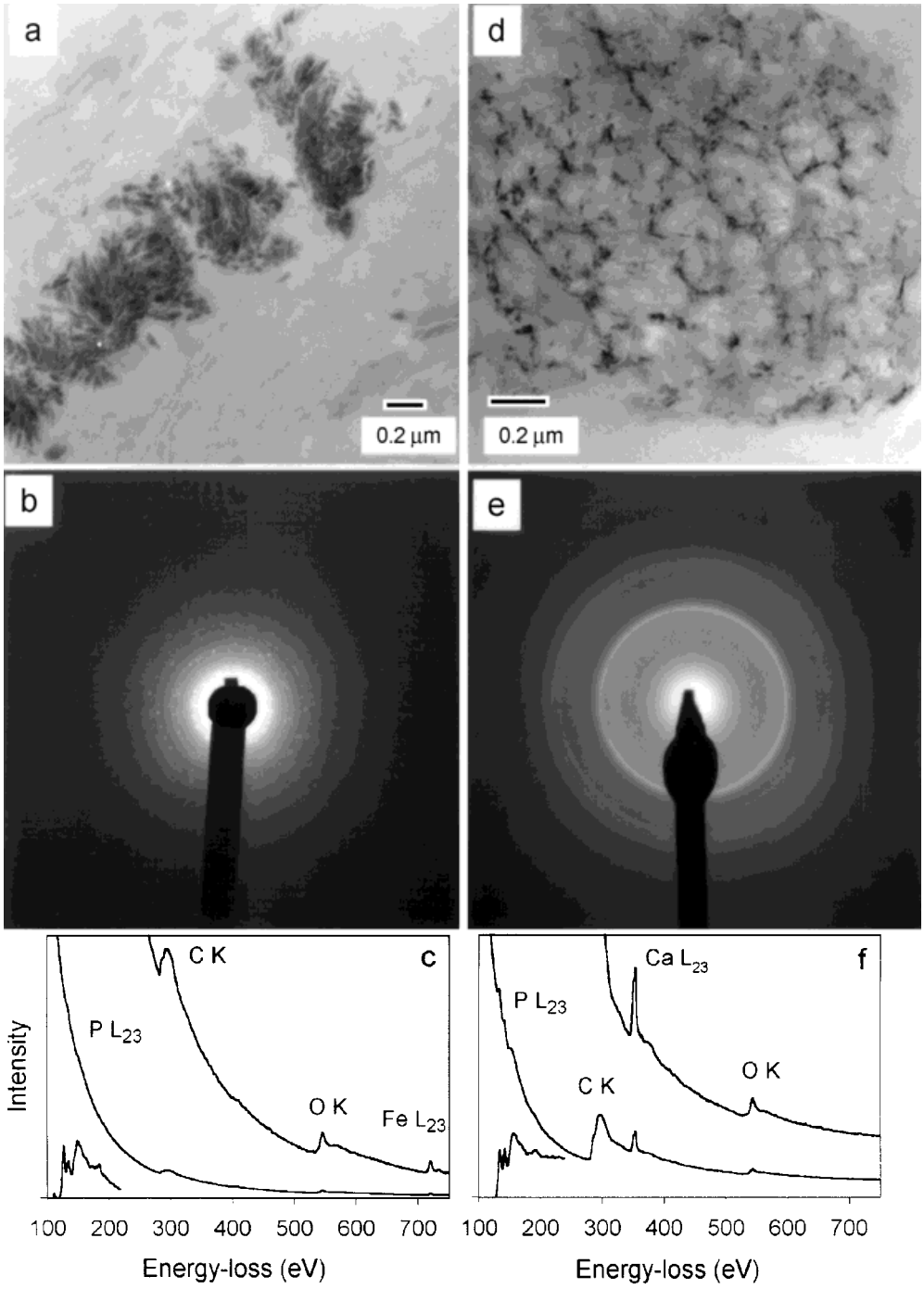

Fig. 6. Identification of deposits in lung tissue located outside of anthracotic areas using TEM. (**a**) Aggregates consisting of small crystals. (**b**) Electron diffraction and the EEL-spectrum (**c**) show that the crystals are vivianite (element-specific ionization edges for P, O, Fe, and C. The background below the P L_{23} edge was subtracted to enhance the visibility of the fine structure typical for phosphates. (**d**) Hexagonally arranged groups of nanometer-sized crystals. (**e**) Electron diffraction and (**f**) the EEL spectrum show that the crystals are hydroxyapatite (element-specific ionization edges for P, C, Ca, and O); the background below the PL_{23} edge is again subtracted and the net edge is shown on the left side of the spectrum.

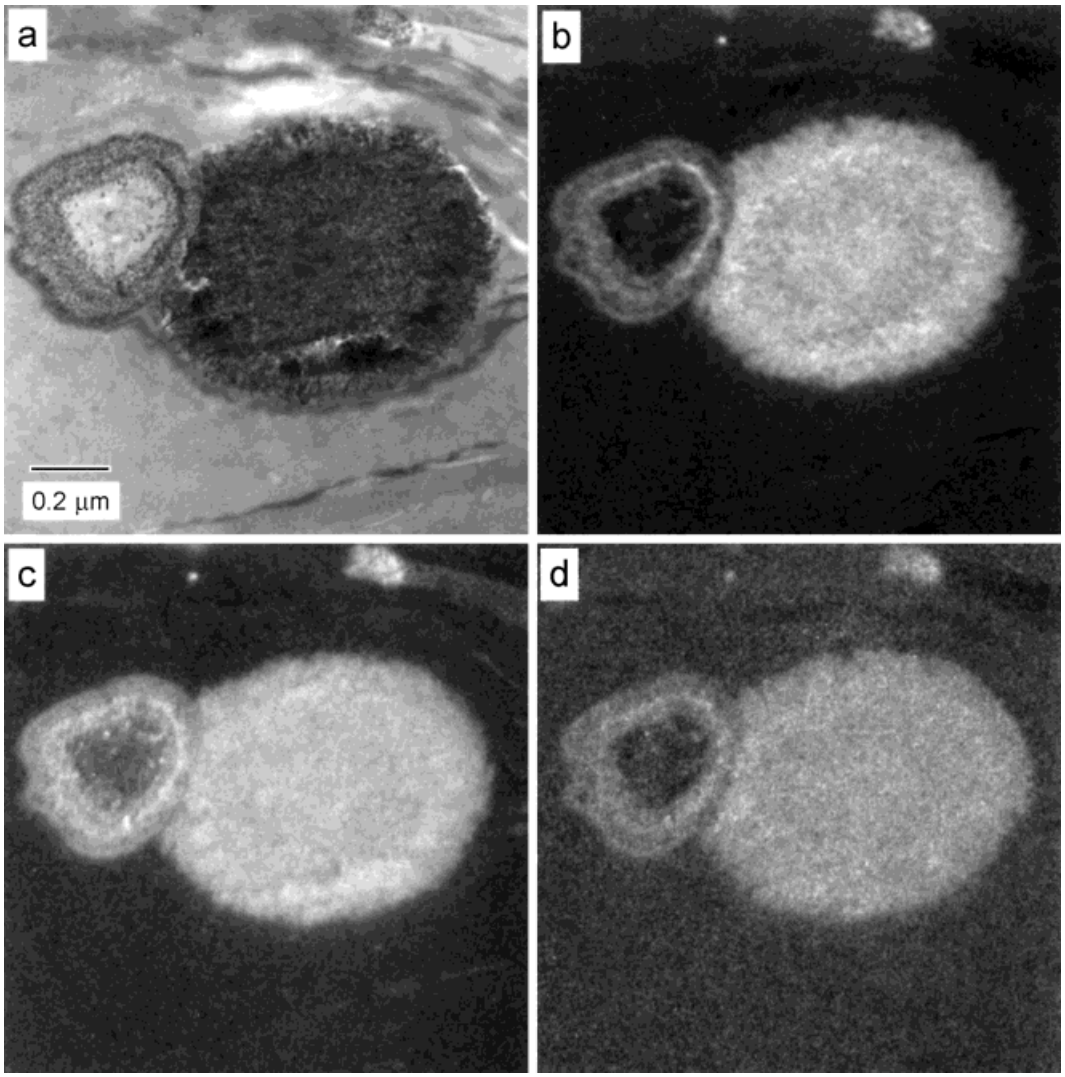

Fig. 7. Nanometer-sized hydroxyapatite crystal aggregates located outside of anthracotic areas, arranged in dense aggregates and in ring-like structures. They were characterized using the elemental mapping technique of energy-filtering TEM. (**a**) TEM bright field image. (**b**) Calcium elemental map. (**c**) Phosphorus elemental map. (**d**) Oxygen elemental map.

ally, hydroxyapatite crystals were found in ring-shaped structures (Fig. 7) of up to 2–3 µm in diameter, but here occurring in the form of round nanometer-sized crystals, which are arranged in concentric layers. The elemental maps shown in Figure 7 reveal that the visible crystals are all hydroxyapatites. The ring seems to fill from the outside to the center. The "lumen" of the ring is filled with an electron-lucent organic material containing carbon and oxygen.

DISCUSSION

Humans have long been exposed to air pollution. As long as 5,300 years ago the Tyrolean Iceman was already inhaling different kinds of dust. Particulate carbon, most probably from open indoor fires, was mainly

responsible for the anthracotic areas in his lung. Lungs of mummies from different climatic conditions, from different epochs and mummified in different ways, have been found to have anthracotic areas in their lungs (Brothwell et al., 1969; Zimmerman, 1981; Walker et al., 1987; Ascenzi et al., 1996; Hart Hansen and Nordqvist, 1996; Wang, 1996; Zimmerman, 1996). In Egyptian mummies (Walker et al., 1987) and in mummies from Xinjiang (China) (Wang, 1996) not only soot particles but also double-refracting crystals were identified in the polarizing microscope, and dust analyses showed that these crystals were silicates, which were believed to derive from eolian sands (Wang, 1996).

As in Egyptian and Chinese mummies, mineral crystals were also detected in the lungs of the Tyrolean Iceman, in the anthracotic areas between the plentiful soot particles. It is not surprising to find muscovite crystals, as the Ötztal Alps, the part of the Central Alps where the Iceman was found and where he probably lived, are composed of muscovite-bearing metamorphic rocks, including large amounts of paragneiss and schists with intercalated muscovite granite-gneiss and two-mica augen-gneiss (Purtscheller, 1971; Oberhauser, 1980). Mica-rich rocks are known to weather easily (Purtscheller, 1971) so that muscovite crystals, which are relatively resistant to weathering, come free. As muscovite is able to cleave to fine plates, the smallest crystals easily become airborne and then may be inhaled. Some of these crystals could come directly from stones in the fireplace, where the heat might liberate them. It is known that macrophages in the lung alveoli are able to ingest this material and they are either coughed up with ingested material or deposited in the connective tissue of the lung. As there are a lot of muscovite crystals in the Iceman's lung tissue and because the inhaled material presumably came from his living environment, he may have lived in an area with mica- (muscovite-) rich rocks. The illite particles could refer to a muscovite-rich area too, as illite is a hydromica and derives mainly from muscovite by partial hydrolysis, e.g., in mica schist (Rösler, 1984). From the anthropological and archaeological points of view, the Tyrolean Iceman may have come from the Vintschgau, the east-west Etsch valley south of the Hauslabjoch (Spindler, 1995), probably from the area of Naturns (Barfield et al., 1992), where Late Neolithic settlements have been found. This is an area with muscovite granite-gneiss and two-mica augen-gneiss occurrences nearby. Such rocks contain an abundance of muscovite.

Because of their composition of carbon and oxygen, and sometimes silicon, the amorphous organic particles in the Iceman's lungs could derive from plant cell wall material. The latter is partly indigestible by alveolar macrophages because human beings do not have enzymes to digest special plant cell wall materials. These could then be deposited in the anthracotic areas like inorganic material. The particles no longer exhibit special cell wall structures, but this could be due to the long storage or partial digestion by the macrophages. This organic material in the lungs could be threshing residues, as botanical analyses of the Iceman's fur clothing revealed two grains of one-grained wheat (*Triticum monococcum)* still in the husks (Bortenschlager et al., 1992), and threshed fragments of the same wheat and of *Triticum sp.* were found in his birch-bark vessel (Spindler, 1992). Cell wall material with similar composition to that in the lungs of the Iceman was also detected in recent wheat threshing residues (Pabst and Hofer, unpublished). These results give further support to Spindler's (1996) assumption that the Iceman at least occasionally was in contact with a grain-growing community. He could have helped to harvest and thresh the grain before leaving the community for the high mountains, where he may have died in autumn because of an early onset of winter (Spindler, 1996).

As vivianite and hydroxyapatite are found outside the anthracotic areas, we assume that these crystals were not inhaled but were crystallized after the death of the Tyrolean Iceman. Vivianite is also known to be formed in fossil bones and teeth (Gmelin, 1965). Vivianite has crystallized not only in the lungs but also in some areas on the surface of the Iceman's skin, where blue pustules were described (Tiefenbrunner.

1992). These were interpreted as air-oxidized vivianite, possibly crystallized on contact regions between the body surface and iron-containing material, an interpretation that was recently verified by chemical analyses (Tessadri, 1998). Additionally, iron and phosphate were found using x-ray microanalysis in ultrathin sections of the Iceman's skin (Van der Velden, 1995).

When the Iceman was found in a rock hollow he was partly lying in melted ice (Henn, 1992). As the discovery site in fact consists of iron-containing para/ortho-gneiss (Tessadri, 1998), leached iron ions in the melted ice may have entered the Iceman's lungs through his mouth. The phosphate may derive from excrement. The rock hollow where the Iceman was found seems to be an ideal place for humans and animals to shelter, and recently chamois and semi-wild sheep were seen there (A. Lippert and G. Patzelt, personal communications) and left excrement. Additional excrement in the hollow comes from large flocks of sheep that for centuries, perhaps even in the Iceman's time, were driven in the spring from the Vintschgau through the Schnalstal and over passes to the meadows of the northern Ötztal and its side valleys and were driven back in autumn (Spindler, 1995). There was also excrement at the site which may derive from the Late Neolithic (Barfield et al., 1992) along with a few old bones. Excrement and bones are rich in phosphates, which may have mixed into the melted ice. During the 5,300 years that the Iceman lay in state in the Ötztal Alps, the glacier advanced and receded several times (Spindler, 1995). Probably there were times when the Iceman lay in a slush of ice and water, then underwent freeze-drying when the temperature dropped. Such conditions would have permitted crystallization of the phosphates.

Since iron and phosphates are components of the human body as well, it is also possible that these mineral crystals may have originated in the Iceman's own body.

Apatite crystals similar to those we found in the Tyrolean Iceman have also been reported in an Alaskan mummy (Zimmerman et al., 1971). The hydroxyapatite crystals in the Iceman could derive from calcium and phosphates from the above-described excrement or bones, as is known from areas with guano deposits (Gmelin, 1965). Calcium could also come from weathered feldspar at the site, or could have come from endogenous calcium and phosphates in the Iceman's body. Further evidence of a secondary crystallization of hydroxyapatite is given by x-ray microanalysis of the Iceman's skin (Van der Velden et al., 1995), where calcium phosphate was also detected.

In conclusion, it can be said that the lungs of the Tyrolean Iceman contain inorganic and organic materials that were inhaled and so deposited during his lifetime; these materials tell us something about his environment and his work. On the other hand, his lungs provide evidence of secondary crystallization that occurred during his 5,300 years of storage high in the mountains.

ACKNOWLEDGMENTS

For the opportunity to do this study we thank the Forschungsinstitut für Alpine Vorzeit, Innsbruck, especially W. Platzer and O. Gaber for information pertaining to this work. We thank G. Dohr (Inst. für Histologie and Embryologie) for making contacts and helpful discussions, A. Fenninger (Inst. für Geologie und Paläontologie), M. Gailhofer (Inst. für Pflanzenphysiologie), G. Reibnegger (Medizinisch-Chemisches Institut) (all Univ. of Graz), K. Stattegger (Inst. für Geologie, Univ. Kiel), F. Purtscheller and P. Mirwald (Inst. für Mineralogie und Petrographie, Univ. Innsbruck), and A. Lippert (Inst. für Ur-und Frühgeschichte, Univ. Wien), G. Patzelt (Inst. für Hochgebirgsforschung) for discussion and helpful suggestions, K. Irgolic for providing research material, and E. Schöninkle and A. Blaschitz for technical assistance.

LITERATURE CITED

Ascenzi A, Bianco P, Nicoletti R, Ceccarini G, Fornaseri M, Graziani G, Giuliani MR, Rosicarello R, Ciuffarella L, and Granger-Taylor H (1996) The roman mummy of Grottarossa. In Spindler K, Wilfing H, Rastbichler-Zissernig E, zur Nedden D, Nothdurfter H (eds): Human Mummies (The Man in the Ice, Vol. 3). Wien: Springer, pp 83–92.

Barfield L, Koller E, and Lippert A (1992) Der Zeuge aus dem Gletscher. Wien, Ueberreuter.

Berger A and Kohl H (1993) Optimum imaging parameters for elemental mapping in an energy filtering transmission electron microscope. Optik *92:*175–193.

Bortenschlager S, Kofler W, Oeggl K, and Schoch W (1992) Erste Ergebnisse der Auswertung der vegetabi-

lischen Reste vom Hauslabjochfund. In Höpfel F, Platzer W, Spindler K (eds): Der Mann im Eis, Vol 1. Innsbruck: University of Innsbruck, pp 307–320.
Brothwell DR, Sandison AT, and Gray PHK (1969) Human biological observations on a Guanche mummy with anthracosis. Am. J. Phys. Anthropol. *30:*333–347.
Cliff G and Lorimer GW (1975) The quantitative analysis of thin specimens J. Microsc. *103:*203–215.
De Ruijter WJ (1995) Imaging properties and applications of slow-scan CCD cameras suitable for electron microscopy. Micron *26:*247–276.
Egerton RF (1996) Electron Energy-Loss Spectroscopy in the Electron Microscope. New York: Plenum Press.
Egg M (1992) Zur Ausrüstung des Toten vom Hauslabjoch, Gem. Schnals (Südtirol). In Hüpfel F, Platzer W, Spindler K (eds): Der Mann im Eis, Vol. 1. Innsbruck: University of Innsbruck, pp 254–272.
Gmelins Handbuch der Anorganischen Chemie, A (1965) Weinheim/Bergstraβe: Verlag Chemie GmbH.
Gothe R and Schöl H (1992) Hirschlausfliegen (Diptera, Hippoboscidae: Lipoptena cervi) in den Beifunden der Leiche vom Hauslabjoch. In Höpfel F, Platzer W, Spindler K (eds): Der Mann im Eis, Vol 1. Innsbruck: University of Innsbruck, pp 299–306.
Groenman van Waateringe W (1995) Pollenanalyse als Indikator für das Gerbeverfahren bei den Tierfellen des Mannes vom Tiesenjoch. In Spindler K, Rastbichler-Zissernig E, Wilfing H, zur Nedden D, Nothdurfter H (eds): Der Mann im Eis, Neue Funde und Ergebnisse (The Man in the Ice, Vol. 2). Wien: Springer, pp 67–70.
Gubbens AJ and Krivanek OL (1993) Applications of a post-column imaging filter in biology and materials science. Ultramicroscopy *51:*146–159.
Hart Hansen JP and Nordqvist J (1996) The mummy find from Qilakitsoq in northwest Greenland. In Spindler K, Wilfing H, Rastbichler-Zissernig E, zur Nedden D, Nothdurfter H (eds): Human Mummies (The Man in the Ice, Vol. 3). Wien: Springer, pp 107–121.
Henn R (1992) Auffindung und Bergung der Gletscherleiche im Jahre 1991. In Höpfel F, Platzer W, Spindler K (eds): Der Mann im Eis, Vol 1. Innsbruck: University of Innsbruck, pp 88–91.
Hofer F (1991) Determination of inner-shell cross-sections for EELS-quantification. Microsc. Microanal. Microstruct. *2:*215–230.
Hofer F and Golob P (1987) New examples for near-edge fine structures in electron energy-loss spectroscopy. Ultramicroscopy *21:*379–384.
Hofer F and Pabst MA (1998) Characterization of deposits in human lung tissue by a combination of different methods of analytical electron microscopy. Micron *29:*7–15.
Hofer F, Warbichler P, and Grogger W (1995) Imaging of nanometer-sized precipitates in solids by electron spectroscopic imaging. Ultramicroscopy *59:*15–31.
Johnson DE (1979) Energy-loss spectrometry for biological research. In Hren JH, Goldstein JI, Joy DC (eds): Introduction to Analytical Electron Microscopy. New York: Plenum Press, pp 245–258.
Kothleitner G (1996) Beiträge zur quantitativen Nanobereichsanalytik mittels EELS und EFTEM im TEM. PhD Thesis, Graz University of Technology, Graz, Austria.
Krivanek OL, Gubbens AJ, and Dellby N (1991) Developments in EELS instrumentation for spectroscopy and imaging. Microsc. Microanal. Microstruct. *2:*315–332.
Krivanek OL, Gubbens AJ, Dellby N, and Meyer CE (1992) Design and first applications of a post-column imaging filter. Microsc. Microanal. Microstruct. *3:*187–199.
Krivanek OL, Gubbens AJ, Kundmann MK, and Carpenter GC (1993) Elemental mapping with an energy-selecting imaging filter. In Bailey GW, Rieder CL (eds): Proc. 51st EMSA Meeting. San Francisco: San Francisco Press, pp 586–587.
Lippert A and Spindler K (1991) Die Auffindung einer frühbronzezeitlichen Gletschermumie am Hauslabjoch in den Ötztaler Alpen (Gem. Schnals). Archäologie Österreichs *2:*11–17.
Oberhauser R (1980) Der Geologische Aufbau Österreichs. Wien: Springer.
Purtscheller F (1971) Ötztaler und Stubaier Alpen. Berlin, Stuttgart: Gebr. Bornträger.
Seidler H, Bernhard W, Teschler-Nicola M, Platzer W, zur Nedden D, Henn R, Oberhauser A, and Sjovold T (1992) Some anthropological aspects of the prehistoric Tyrolean Ice Man. Science *258:*455–457.
Rösler HJ (1984) Lehrbuch der Mineralogie. Leipzig, VEB Deutscher Verlag für Grundstoffindustrie.
Spindler K (1992) Der Mann im Eis. Sandoz Bulletin 99.
Spindler K (1995) Der Mann im Eis. München, Goldmann.
Spindler K (1996) The iceman's last weeks. In Spindler K, Wilfing H, Rastbichler-Zissernig E, zur Nedden D, Nothdurfter H (eds): Human Mummies (The Man in the Ice, Vol. 3). Wien: Springer, pp 249–263.
Tessadri R (1998) Vivianite from the iceman of the Hauslabjoch (Tyrol, Austria): Mineralogical-chemical data. In Bortenschlager S (ed): Biogenous Finds Discovered Along with the Iceman (The Man in the Ice, Vol. 4). Wien: Springer.
Tiefenbrunner F (1992) Bakterien und Pilze, ein Problem für unseren ältesten Tiroler? In Höpfel F, Platzer W, Spindler K (eds): Der Mann im Eis, Vol. 1. Innsbruck: University of Innsbruck, pp 100–107.
Van der Velden E, den Dulk L, Leenders H, Dingemans K, van der Bergh M, Weerman M, van der Putte S, Vuzevsky V, and Naafs B (1995) The decorated body of the man from Hauslabjoch. In Spindler K, Rastbichler-Zissernig E, Wilfing H, zur Nedden D, Nothdurfter H (eds): Der Mann im Eis, Neue Funde und Ergebnisse (The Man in the Ice, Vol. 2). Wien: Springer, pp 275–278.
Walker R, Parsche F, Bierbrier M, and McKerrow JH (1987) Tissue identification and histologic study of six lung specimens from Egyptian mummies. Am. J. Phys. Anthropol. *72:*43–48.
Wang BH (1996) Excavation and preliminary studies of the ancient mummies of Xinjiang in China. In Spindler K, Wilfing H, Rastbichler-Zissernig E, zur Nedden D, Nothdurfter H (eds): Human Mummies (The Man in the Ice, Vol. 3). Wien: Springer, pp 59–69.
Williams DB (1987) Practical Analytical Electron Microscopy in Materials Science, 2nd ed. Mahwah, NJ: Philips Electron Optics Publishing Group.
Wininger J (1995) Die Bekleidung des Eismannes und die Anfänge der Weberei nördlich der Alpen. In Spindler K, Rastbichler-Zissernig E, Wilfing H, zur Nedden D, Nothdurfter H (eds): Der Mann im Eis, Neue Funde und Ergebnisse (The Man in the Ice, Vol. 2). Wien: Springer, pp 119–187.
Zimmerman MR (1996) Mummies of the Arctic regions. In Spindler K, Wilfing H, Rastbichler-Zissernig E, zur Nedden D, Nothdurfter H (eds): Human Mummies (The Man in the Ice, Vol. 3). Wien: Springer, pp 83–92.
Zimmerman MR, Yeatman G, and Sprinz H (1971) Examination of an Aleutian mummy. Bull. NY Acad. Med. *47:* 80–103.
Zimmerman MR, Trinkaus E, LeMay M, Aufderheide AC, Reyman TA, Marrocco GR, Ortel RW, Benitez JT, Laughlin WS, Horne PD, Schultes RE, and Coughlin EA (1981) The paleopathology of an Aleutian mummy. Arch. Pathol. Lab. Med. *105:*638–641.
Zissernig E (1992) Der Mann vom Hauslabjoch. Von der Entdeckung bis zur Bergung. In Höpfel F, Platzer W, Spindler K (eds): Der Mann im Eis, Vol. 1. Innsbruck: University of Innsbruck pp 234–244.